Non-equilibrium excitation of CO_2 in an atmospheric pressure helium plasma jet

T. Urbanietz, M. Böke, V. Schulz-von der Gathen, A. von Keudell

Research Department Plasmas with Complex Interactions, Experimental Physics II - Reactive Plasmas, Ruhr-Universität Bochum, D-44780 Bochum, Germany

E-mail: Achim.vonKeudell@rub.de

Abstract. The energy efficient excitation of CO_2 in atmospheric pressure plasmas may be a method to generate solar fuels from renewable energies. This energy efficiency can be very high, if only specific states of the molecules in the plasma are populated creating a strong non-equilibrium. This requires a specific design of the plasma source, method of plasma excitation and choice of gases and admixtures. In this paper, non-equilibrium excitation and dissociation of CO_2 in an atmospheric pressure helium RF plasma jet is analysed for varying absorbed plasma power and admixture levels of CO_2. The concentrations of CO_2 and of CO, as well as the vibrational and rotational temperatures of the possible degrees of freedom of the molecules are evaluated by Fourier transform infrared spectroscopy (FTIR). The molecular rotational vibrational spectra are modelled based on Maxwell-Boltzmann state populations using individual temperatures for each degree of freedom. A strong non-equilibrium excitation of CO_2 and CO has been found. Whereas the rotational temperatures are 400 K or below, the vibrational temperature for CO reaches values up to 1600 K and that of the asymmetric vibration of CO_2 of 700 K. The dependence of these excitation temperatures on plasma power and admixture level is rather weak. The mass balance, the energy and conversion efficiency are consistent with a very simple chemistry model that is dominated by CO_2 dissociation via Penning collisions with helium metastables. A conversion efficiency up to 30 % and an energy efficiency up to 10 % is observed in the parameter range of the experiment.

1. Introduction

At present, the advent of renewable energies from e.g. windmills or biomass creates an urgent demand for decentralized methods to store electrical energy. The direct storage of electricity in batteries on a large scale is hampered by the limited availability of natural resources such as lithium. Therefore, alternative storage solutions based on the conversion of electrical energy into chemical energy are currently explored. In a first step, a given precursor molecule is dissociated by investing a specific reaction enthalpy. In a second step, this energy per molecule is harvested at a later stage in a simple combustion or in a fuel cell to generate electricity on demand. In this context, electricity can be used as energy source for the first step either for (i) *pyrolysis* - dissociation of a gas by simple electrical heating; (ii) for *electrolysis* - dissociation of molecules at a liquid solid interface in an electrochemical cell powered by a specific overvoltage; (iii) for *plasmolysis* - dissociation of a precursor gas in a plasma generated by electric fields. Typical feed gases or liquids for chemical energy storage solutions are N_2, CO_2, or water. All three methods exhibit different advantages and disadvantages in terms of energy and conversion efficiency, scale-up to the industrial size, and flexibility in terms of system size. The energy efficiency represents the most crucial performance parameter, since the specific energy input (SEI) per molecule should be as close as possible to the reaction enthalpy to assure an optimum energy efficient conversion process. In plasmolysis, the energy efficiency may reach theoretically very high values, because only specific degrees of freedoms that are necessary for dissociation may be excited due to the non-equilibrium nature of plasmas. In case of for example CO_2 dissociation, the thermal cracking to CO at 3000 K exhibits an energy efficiency of 55 %. Any higher efficiency of a plasma based process would be advantageous.

In recent years, many groups focused their attention on splitting CO_2 using DBDs, ICPs, gliding arcs, or microwave plasmas [1, 2, 3]. All these discharges have different advantages and disadvantages with respect to energy and conversion efficiency and scalability. For example, DBDs exhibit usually a poor energy efficiency due to the high electric fields involved in plasma generation, but can be scaled up very easily. In contrast, microwave plasmas exhibit better energy and conversion efficiency, but are more difficult to scale up on the industrial scale. Recent experiments using microwave plasmas showed that the neutral gas temperature reaches values of 3000 K to 6000 K inducing a thermal equilibrium that favours CO + O over CO_2 [4]. Microwave plasmas, however, may also be energy efficient for CO_2 conversion at much lower gas temperatures, if one assures a non-equilibrium excitation of only the vibrational states of CO_2 via the so-called vibrational pumping. Fridman et al. [5, 6] demonstrated such non-equilibrium excitation of CO_2 in a microwave plasma exciting a supersonic flow of CO_2. Due to the supersonic flow, the residence time of the molecules in the hot plasma zone is very small and the back reaction from CO and O_2 to CO_2 is suppressed due to efficient vibrational translational relaxation. So far a high energy and conversion efficiency of up to 85% found in these experiments [5, 6] could not be reproduced in the

scientific community up to now.

To expand the possible applications of plasmolysis, the combination of plasmas with catalysts is often investigated [7, 8, 9]. Various synergisms have been observed, which may originate from the impact of the plasma on the catalyst by avoiding any poisoning, providing internally excited molecules or from the impact of the catalyst on the plasma by enhancing electric field strengths. The combination of plasma and catalyst allows for more flexible gas mixtures to be treated and more flexible operating windows for the catalyst temperature. The exact identification of the synergism in plasma catalysis is, however, very difficult due to the intimate coupling between plasma and surface. Any plasma catalysis experiment is always hampered by the fact that the inherent power dissipation in the plasma may also heat the gas and the topmost surface of the catalyst. Thereby, any plasma enhancement of the reaction rate may be simply caused by a plasma induced heating of the catalyst surface.

The first step in the exploitation of any non-equilibrium in atmospheric pressure plasmas is, however, the design and development of robust excitation schemes that populate only specific degrees of freedom of the molecules of interest in the plasma. The most straightforward method would be laser excitation of specific states, as it occurs in any CO_2 laser. In comparison to plasma methods for CO_2 conversion, however, the overall energy efficiency of such a laser induced conversion is much smaller due to the low efficiency of the laser light generation itself. In this paper, we attempt to generate a non-equilibrium plasma excitation of CO_2 diluted in a fast flow of helium. This may allow an independent control of the gas temperature that is dominated by the high flow of the feed gas combined with the selective excitation of the molecules by low energy electrons or by Penning collisions with the excited noble gas atoms or dimers. As a plasma source, we use an RF driven plasma jet with plane parallel electrodes. Such plasma sources are extensively investigated with respect to their plasma physics and chemistry for various mixtures of noble gases and molecules [**?**, 10, 11, 12].

2. Experiment

2.1. Experimental Setup

A scheme of the experimental setup is shown in Fig. 1 as cross section along the gas flow (a) and a cross section at the FTIR measurement position (b). The plasma chamber consists of an aluminium body in which two electrode holders are inserted from the top and the bottom. The electrodes consist of an aluminium support, a macor insulation layer and a copper electrode. The 0.5 mm thick copper electrode (26 mm × 13 mm) is protected by a 1 mm thin glass layer as a dielectric barrier to suppress any unintentional arcing at very high plasma powers that may damage the setup. This confines a plasma volume of 26 mm × 13 mm × 1 mm. The plasma volume is located in a central section within a rectangular gas channel with an extension of 54 mm × 14 mm × 1 mm. The plasma gas is fed at the beginning of the rectangular gas channel and is guided to an

exhaust at the end. The position along the gas channel are denoted as x, with the beginning of the plasma at $x = 14$ mm. The plasma volume is observed in transmission with an optical path either along the gas flow using KBr end windows or perpendicular to the gas flow at the centre ($x = 27$ mm) of the discharge using KBr side windows. A 4 mm gap between the plasma and the KBr side windows exists to avoid any direct contact of the plasma with the KBr window material. This gap (sketched as dashed rectangle in Fig. 1a) extends 30 mm along the 26 mm plasma channel with a height of 15 mm. The plasma gas can only interact with the trapped gas in this gap volume via the long side of the gas channel with a boundary area of 30 mm × 1 mm.

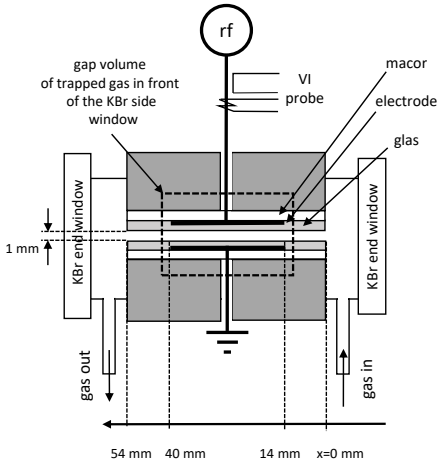

Figure 1. Cross section of the experimental setup along the gas flow. The plasma volume (26 mm × 13 mm × 1 mm) is confined by the two electrodes. The plasma is powered at 13.56 MHz by the RF generator attached to one electrode via a matching network. The IR beam path samples the plasma composition at the central position.

The plasma forming gas consists of helium at a flow of 2 slm with a variable admixture of CO_2 at a flow between 5 sccm and 20 sccm. Since the flow of helium is so much larger than the flow of CO_2, an efficient and fast gas mixing is assured by injecting the helium directly in front of the CO_2 flow controller against the CO_2 flow direction. This mixing procedure results in a very stable CO_2 admixture in the helium flow after a few seconds of switching the CO_2 flow on.

The plasma is powered by a 13.56 MHz power supply connected to one of the electrodes via a matching network. The other electrode is grounded. The actual absorbed power in the plasma is measured using a VI probe in the RF power line. By measuring the phase shift between voltage and current, the actual absorbed power in the plasma is calculated by comparing the response of the setup with and without plasma. This yields values in the range of a few Watt, as being typical for atmospheric pressure non-equilibrium RF plasma jets [10].

2.2. Infrared spectroscopy

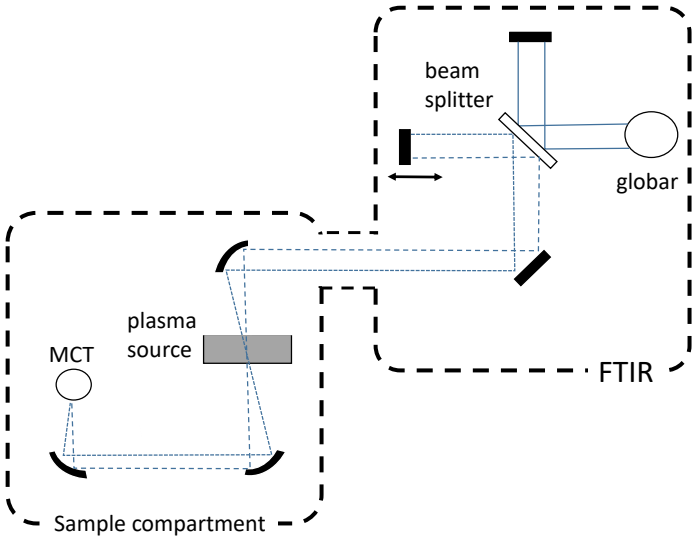

Figure 2. Experimental Setup of the FTR beam path.

The plasma chemistry is monitored by a Bruker IFS 66 FTIR spectrometer using an external MCT detector (see Fig. 2). The parallel beam from the spectrometer is focused in the plasma channel using off-axis parabolic mirrors with a focal length of 150 mm. The complete beam path is purged with nitrogen gas. For each spectrum 100 scans at a wavenumber resolution of nominal 0.3 cm^{-1} are taken. The path length in between the KBr windows is 22 mm in total consisting of 14 mm in the gas channel and two times a path length of 4 mm within the gap volume in front of the two KBr side windows. The path length in between the electrodes passing the plasma is 13 mm (see Fig. 1b).

The sampling of the CO_2 concentration in the narrow gap in between the electrode requires a focussing of the IR beam. This has the disadvantage that the number of sampled molecules within the beam volume is much smaller compared to a typical parallel beam transmission measurement. For example, if one compares a perfectly focussed beam with a parallel beam, the ratio of sampled volumina is 1:3, equivalent to the ratio between a cone and a cylinder with the same height. Consequently, there is a trade-off in our experiment between a perfectly focussed beam to guide the IR beam through the gap in between the electrodes to enhance signal quality and an only moderate focus to enhance the signal by sampling more molecules in the beam volume. This trade-off is adjusted experimentally by varying the aperture of the infrared source in the spectrometer, yielding an optimum diameter of 4 mm. This is imaged within the electrode gap to a beam waist with a diameter of 5 mm. This dimension is larger than the electrode gap, so that the IR beam volume is more determined geometrically by the

edges of the electrode mounting rather than the optics of the focussing. From these geometric constraints, we can construct a wedge shaped beam volume, as illustrated in Fig. 3, yielding a beam focus in the center in between the electrodes with an extension of 5 mm along the electrodes in x-direction and only 0.1 mm in the z-direction.

The analysis of the absorption using the Lambert Beer law is based on a parallel beam passing a gas of a specific density. When using a focussed or divergent beam, the sampled volume has to be corrected for the same transmitted length. For this, we separate the sampled IR beam volume in Fig. 3 into a *sampling volume side* $V_{IR,side}$ to account for the transmission in the gap volume in front of the KBr side windows and a *sampling volume central* $V_{IR,central}$ to account for the transmission in the space in between the electrodes. For both wedge shaped volumina with an extension of 5 mm along the x-axis and a cross section in the y,z-plane as indicated in Fig. 3, we can calculate the correction factors when compared to a cubus V_{cubus}, yielding 0.83 for $V_{IR,side}$ /$V_{cubus,side}$ and 0.55 for $V_{IR,central}/V_{cubus,central}$. These correction values need to be weighted with the length of both volumina along the IR beam path, yield an overall correction value of 0.65. Based on this rough estimate, any transmission measurement using the optical beam path samples only 65% of the molecules compared to a parallel optical beam path.

This correction is tested in our experiment by quantifying the absorption of 0.5% admixture of CO_2 in 1 bar He. This yields, a CO_2 density of only 9×10^{22} m^{-3} although 0.5% corresponds to a density of 1.2×10^{23} m^{-3} equivalent to an experimental correction value of 0.75 which is in reasonable agreement with the estimated factor of 0.65 above. This correction procedure has also been tested by filling the gap volume with KBr transparent material. In this configuration the experimental correction factor yielded a lower value of 0.5, which is also consistent with the estimated factor 0.55 from the ratio $V_{IR,central}/V_{cubus,central}$ only.

These corrections based on the sampled volumes, however, have also an impact on the absolute scale of dissociation degrees that can be measured. From the analysis of the flow pattern of helium and CO_2 in our experiment (discussed below), we can deduce that a significant fraction of the gas streamlines passes the gap volume, where no plasma is excited and only a fraction passes the electrode gap. If we assume, that 100 % dissociation is reached by plasma conversion of CO_2 into CO, the measurement would still yield a lower value, because CO_2 is always sampled in $V_{IR,side}$: if we compare this $V_{IR,central}$ with the total IR beam volume ($V_{IR,central} + V_{IR,side}$) corresponding to the base line measurement of CO_2 before the plasma is ignited, one obtains a ratio of 43.5%. Consequently, even 100% dissociation within the plasma will cause only a decrease in the CO_2 signal sampled by the IR beam of 43.5%.

2.3. Data evaluation

The detection of the excitation of molecules is often performed by analyzing the overtones of the vibrations and plotting the line intensities on a Boltzmann plot [13, 14].

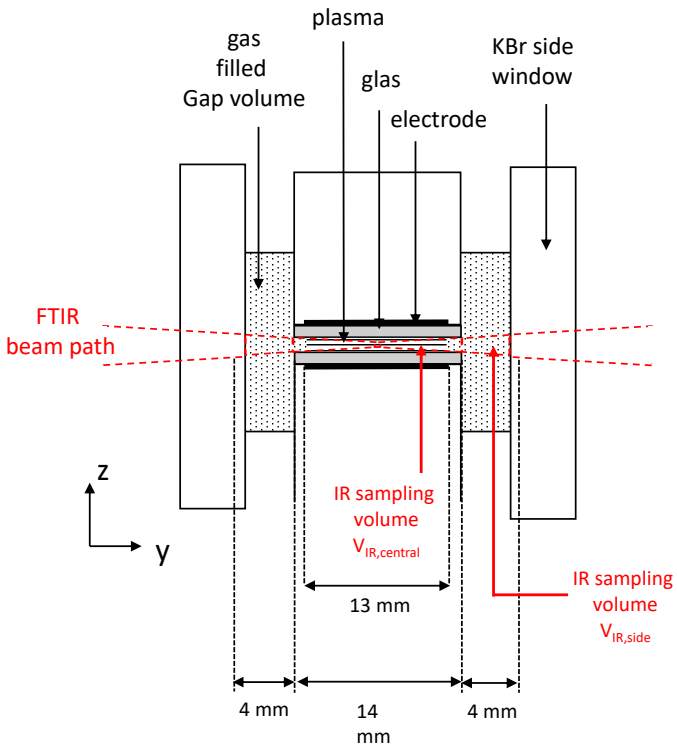

Figure 3. Optical path of the focused IR beam at the measurement position. The IR beam path is determined by the blocking of the beam by the solid electrodes. This defines a wedge shaped volume V_{side} in the gap volume in front of the IR windows and a wedge shaped volume $V_{central}$ in between the electrodes. The extension of these wedges is 5 mm in the x direction.

A unique slope or shape of the distribution of these lines then indicates for example a Boltzmann distribution or a Treanor distribution of the population of the vibrational states. The line strengths of the overtones are usually much weaker than the line strengths of the fundamentals, which can be compensated by using higher concentrations or longer optical paths. These common methods for analysis of vibrational excitation, however, are not easily applicable for non equilibrium atmospheric pressure plasmas generated in small discharge gaps: due to geometric constraints, the optical path lengths is limited to a few centimetre at most; the admixture of CO_2 need to remain in the percent range, because the plasma becomes unstable at higher admixture levels.

The excitation and dissociation of CO_2 and CO is monitored by evaluating the ro-vib transitions of the fundamentals of the stretching vibrations at ν_1 =2149 cm^{-1} of CO and the asymmetric stretching vibrations at ν_3 = 2340 cm^{-1} of CO_2. For the modelling of the IR absorption spectra, the transitions at wavenumbers ν_{ij} with the corresponding Einstein coefficients A_{ij} are taken from the HiTRAN database [15, 16, 17]. The line strengths S_{ij}, however, are calculated by invoking individual distribution functions for the population of each degree of freedom of the molecules such as vibrations and

rotations. The calculation follows the same steps, as shown in detail by Klarenaar et al. [18]. The distribution functions for the different degrees of freedom are estimated using Maxwellians with individual temperatures for each degree of freedom of the molecules. The calculation follows 6 individual steps:

(1 - *rotational distribution*) At first, the rotational distribution function is calculated based on the energy of a rotator for a given rotational quantum number j of:

$$E_{rot} = B \cdot j(j+1) - D \cdot j^2(j+1)^2 + H \cdot j^3(j+1)^3 \tag{1}$$

The degeneration of a particular state j is given as $g_{rot,j} = g_{nuclear} \cdot (2j+1)$. The factor $g_{nuclear}$ accounts for the different multiplicity depending on the nuclear spin. This is equal to unity for molecules consisting of atoms with no nuclear spin, as it is the case for CO and CO_2. The probability p_{rot} of each rotational state, assuming a Maxwellian distribution for this degree of freedom, is defined by a rotational temperature T_{rot}:

$$p_{rot} = \frac{g_{rot,j}}{Q_{rot}} \exp\left(-c_2 \frac{E_{rot,j}}{T_{rot}}\right) \tag{2}$$

$c_2 = hc/k_B$ with h the Planck constant, c the speed of light and k_B the Boltzmann constant. The partition function Q_{rot} is calculated accounting for rotational numbers up to $j = 100$:

$$Q_{rot} = \sum_{j=0}^{j=100} g_{rot,j} \exp\left(-c_2 \frac{E_{rot,j}}{T_{rot}}\right) \tag{3}$$

(2 - *vibrational distribution*) Second, the vibrational distribution of CO_2 is calculated based on the energy of fundamentals of the asymmetric stretching vibration at $\nu_3 = 2349.16\ cm^{-1}$, of the symmetric vibration mode at $\nu_1 = 1333.93\ cm^{-1}$, and of the bending mode at $\nu_2 = 667.47\ cm^{-1}$ [5]. The vibrational distribution of CO is calculated based on the energy of the fundamental of the stretching vibration at $\nu_1 = 2149\ cm^{-1}$ [19]. The probability $p_{vib,i}$ of an individual vibrational mode i with quantum number n_i with an energy in wavenumbers G_i including the centrifugal distortion $\omega_e x_{e,i}$ is:

$$p_{vib,i} = \frac{g_{vib,i}}{Q_{vib,i}} \exp\left(-c_2 \left(n_i \frac{G_i}{T_{vib,i}} - n_i(n_i-1)\frac{\omega_e x_{e,i}}{T_{rot}}\right)\right) \tag{4}$$

with the partition function

$$Q_{vib,i} = \sum_{\nu_i=0}^{30} g_{vib,i} \exp\left(-c_2 \left(n_i \frac{G_i}{T_{vib,i}} - n_i(n_i-1)\frac{\omega_e x_{e,i}}{T_{rot}}\right)\right) \tag{5}$$

The degeneracy of the vibrational modes depends on the type of molecular vibration. For a linear molecule it is equal to unity. For a bending vibration, two symmetry planes exist and depending on the excitation, the two directions might overlap resulting in a degeneracy of $n_i + 1$. The degeneracy for the stretching vibration of CO is $g_{vib,\nu_1} = 1$. The degeneracy for the symmetric and asymmertic stretching vibrations of CO_2 are $g_{vib,\nu_1} = g_{vib,\nu_3} = 1$ and for the bending vibration $g_{vib,\nu_2} = n_2 + 1$. The partition

function for each vibrational mode is again calculated so that the sum of the probabilities equals unity. The total probability for a particular state for a given rotational quantum number j and vibrational quantum numbers n_i is (example for three vibrational states):

$$p_{total,j,\nu_1,\nu_2,\nu_3} = p_{rot,j} \cdot p_{vib,\nu_1} \cdot p_{vib,\nu_2} \cdot p_{vib,\nu_3} \tag{6}$$

(3 - *line strengths*) Third, the line strength S_{lu} for a transition with Einstein coefficient A_{lu} and wavenumber ν_{lu} connecting an upper state u with a lower state l of the molecule with an abundance of $p_{isotope}$ is given as:

$$S_{lu} = p_{isotope} \frac{g_{rot,u} A_{lu}}{8\pi\nu_{lu}^2} \left(\frac{p_{total,l}}{g_{rot,l} g_{vib,l}} - \frac{p_{total,u}}{g_{rot,u} g_{vib,u}} \right) \tag{7}$$

(4 - *line broadening*) These line strengths are then broadened by convoluting them with a normalized line width function f assuming either pressure broadening or Doppler broadening. The line width due to Doppler broadening for gas temperatures of about 400 K in our experiments is in the range of 10^{-6} cm^{-1} and can be neglected in comparison to the other broadening mechanisms. According to the HiTRAN database, elemental data are given for the pressure broadening of each transition assuming collisions with air γ_{air} or with the molecules of interest γ_{self} yielding Lorentzian line widths in the range of 0.1 cm $^{-1}$. The corresponding line width function f with a broadening parameter γ is:

$$f = \frac{1}{2\pi} \frac{\gamma}{(\nu - \nu_0)^2 + \left(\frac{1}{\gamma}\right)^2} \tag{8}$$

The data in the HiTRAN database cover only the quenching of vibrationally excited states via VT relaxation by collisions with air or among the species themselves. The de-excitation of vibrationally excited species by collisions with He or by collisions with the nearby surrounding walls are not accounted for per se. Direct pressure broadening measurements for CO in He and Ar [20, 21] yielded, however, γ values very similar to the γ coefficient for CO in air. We adopted this in our calculation by adjusting the Lorentzian to the the peak shape using an additional factor b to expand the formula $\gamma = \left(\frac{296K}{T}\right)^{n_{air}} \gamma_{self} \cdot b$, with n_{air} taken from the HiTRAN database and T taken as the average temperature of the molecules. The best agreement was found by setting $b = 1.5$.

The wavenumber dependence of the absorption coefficient α is calculated from the line strengths S, the density of species n by the convolution with the line width function f.

$$\alpha = Snf \qquad\qquad [cm^{-1}] \tag{9}$$

(5 - *optical transmission*) The wavenumber dependence of α is used to calculate the transmission following the Lambert-Beers Law:

$$T(\nu) = \frac{I}{I_0} = \exp(-\alpha d) \tag{10}$$

(6 - *instrumental broadening*) Finally, the spectrum $T(\nu)$ is convoluted with a Gaussian to account for the finite resolution of the FTIR spectrometer. For this, the spectra are convoluted with a Gaussian using a width of 0.22...0.3 cm^{-1}. The actual width is extracted directly from the spectra. This fitting is rather robust, because the Gaussian line width from the instrumental broadening and the Lorentzian line width from the pressure broadening lead to a very distinct line shape. The fitting is performed using a χ^2-Fit by varying the temperatures and concentrations of the species. The accuracy of this temperature determination is typically $\Delta T_{vib}\pm$ 100 K and $\Delta T_{rot}\pm$ 20 K. For CO_2 and CO, the lines of the three most abundant isotopes are taken into account.

The accuracy of the FTIR modeling is tested by comparing the predicted line strengths S_{ul} according to eq. 7 with the tabulated values in the HITRAN database for a thermal equilibrium of 300 K. Excellent agreement is found. The simulated FTIR spectra are also directly compared to the simulations of Klarenaar et al. [18] for a specific concentration and temperatures. Both codes agree very well.

The data evaluation so far is based on describing the non-equilibrium by using different temperatures for different degrees of freedom of the molecules, implying a Maxwell-Boltzmann population of the states for each degree of freedom individually. Such a Maxwell-Boltzmann distribution seems to be valid for the rotational degrees of freedom, as indicated by the good agreement between model and spectra presented below. For the vibrational degrees of freedom, however, only the transitions for the vibrational quantum numbers the $0 \rightarrow 1$ and $1 \rightarrow 2$ are mostly visible. Their ratio is expressed nevertheless by a Boltzmann factor for a given temperature, although the population of the states with higher vibrational numbers might deviate from the Maxwell Boltzmann distribution.

2.4. Flow pattern in the measurement cell

The design of our measurement cell implies the formation of a complex flow pattern of 2 slm helium passing the gas channel with the adjacent trapped volumes. This is evaluated based on a COMSOL simulation using incompressible Navier Stokes equations for helium and diffusive-convective transport equations of the admixed 0.1 mol/m^3 CO_2 (equivalent to 0.22%) including a reaction rate for the dissociation of CO_2. The resulting flow pattern of helium is shown in Fig. 4(a) and the concentration of CO_2 in mol/m^3 in Fig. 4b. One can clearly see that a significant fraction of the flow passes the gap volume rather than the plasma channel. The flow velocity decreases inside the gas channel before it accelerates again towards the outlet. The CO_2 flow, added to the helium flow, follows the convective and diffusive transport with the helium flow. The plasma conversion of CO_2 in the region in between the electrodes is mimicked by an overall reaction rate that is adjusted so that a depletion of 40% in the plasma region occurs. As illustrated in Fig. 4b, one can see that most of the CO_2 is converted in the central region, where the flow velocity decreases to 0.5 ms^{-1}. This seems reasonable given the long residence times of

CO_2 in the plasma region. This simulation, also shows that even 100% conversion in the plasma volume does not imply the absence of any CO_2 absorption in the IR beam path due to the presence of CO_2 in the gap volumina. The analysis of the IR detection volume, as discussed above, reveals that even a 100% conversion in the plasma volume corresponds to only a 43.5% reduction in CO_2 absorption.

3. Results

Fig. 5 shows the CO_2 absorption spectrum for an admixture of 0.5% CO_2 to the helium feed gas for an absorbed plasma power of 3 W. The residuum for the difference between model and measurement is below 5% of the maximum absorption. The details of the P and the R branch of the spectrum are shown in Fig. 6. The best fit is reached with a rotational temperature of 400 K and an vibrational temperature for the stretching vibrations around 700 K. The temperature for the bending vibration is 400 K. The CO_2 concentration is 3.7×10^{22} m^{-3}.

A rotational temperature of 400 K is consistent with the thermal management of the plasma source. Such an enhanced rotational temperature may originate from an increased overall temperature of the whole setup. According to the RF power supply readout, 70 W is delivered to the plasma electrodes, but only a few Watts are dissipated in the plasma according to the VI measurements. The remainder is presumably dissipated by stray capacitances in the RF cables and the electrodes leading to an overall heating of the setup to a temperature slightly above room temperature.

The absorption spectrum for CO is shown in Fig. 7 yielding a density of 0.95×10^{22} m^{-3}. The rotational temperature is again 400 K, however, the vibrational temperature is at 1250 K.

The excitation temperatures of CO have been measured for the three admixture levels of 0.25%, 0.5%, and 1% for varying absorbed plasma powers between 0.7 W and 3.5 W, as shown in Fig. 8. The rotational temperature increases almost linearly with varying plasma power. The vibrational temperature is at 1600 K for an admixture level of 0.25 %, it increases from 1200 K to 1400 K with plasma power for an admixture level of 0.5%, and it increases from 800 K to 1000 K with plasma power for an admixture level of 1%. We assume that the vibrational and rotational excitation of CO originates mainly from the dissociation reaction either by direct electron impact of CO_2 or by Penning dissociation between excited helium metastables and CO_2. This electronic energy transfer to CO_2 causes dissociation, creating a highly vibrational excited CO molecule. The momentum transfer from electrons or from helium to CO_2 or to CO is small, so that the excitation of the rotational degrees of freedom is not efficient. The initially excited CO molecules may quench via wall collisions or via collisions with other CO_2 and CO molecules. This may explain, why the highest temperatures are observed for the lowest admixture levels, which reduces the probability to collide with another CO_2 molecule as the most efficient quenching partner. The increase in vibrational temperature with higher plasma powers for higher CO_2 admixture levels may indicate

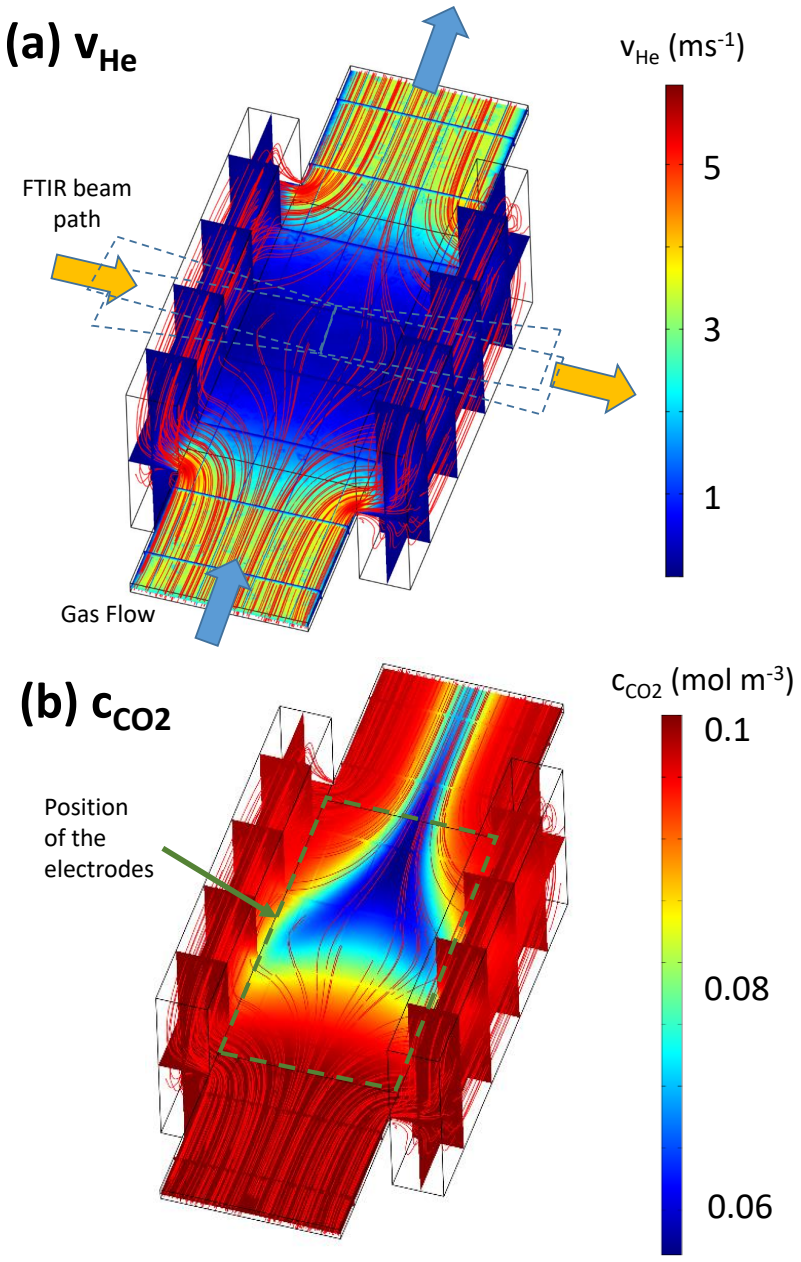

Figure 4. Comsol simulation of the helium velocity (a) and CO_2 concentration (b) pattern through the gas channel and the adjacent trapped volumina in front of the KBr side windows. The red lines denote the streamlines of He and of CO_2 respectively. The direction of the gas flow inlet and outlet, as well as the estimated dimensions of the wedge shaped optical path of the IR sampling beam are indicated.

a contribution of vibrational pumping of the CO_2 molecules prior to electron impact dissociation. Such a process is more efficient at higher plasma powers and at higher admixture levels.

The excitation temperatures of CO_2 have been measured for an admixture level

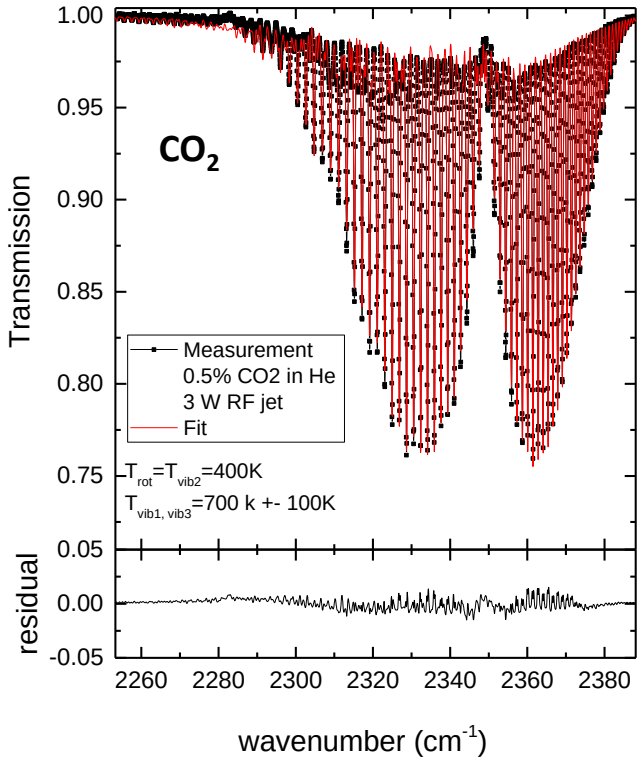

Figure 5. Absorption spectrum for CO_2 in a plasma jet at 3 W absorbed plasma power with 0.5% CO_2 in the feed gas (upper panel). The residuum between measurement and model, the absolute scale corresponds to 20% of the absorption signal (lower panel).

0.25% for varying absorbed plasma powers between 0.7 W and 3.5 W, as shown in Fig. 9. The rotational temperature increases slowly with absorbed plasma power. The vibrational temperature of the bending vibration is similar to the rotational temperature. The vibrational temperatures of the symmetric and asymmetric stretching vibrations are in the range between 500 K and 800 K with no clear trend. The excitation of CO_2 originates mainly from the direct electron impact excitation, by Penning excitation in collisions with helium metastables, or by vibrational pumping during collisions among vibrationally excited CO_2 molecules. The electronic energy transfer from electrons or excited helium metastable atoms to CO_2 creates vibrationally excited CO_2 molecules. The momentum transfer from collisions with electrons or helium is small, so that the excitation of the rotational degrees is apparently inefficient. Therefore, a non-equilibrium excitation of CO_2 results.

The vibrational temperature of the stretching vibration of CO_2 is significantly lower than that of CO. One may speculate that the observed vibrational temperature of CO_2 originates from an average of the vibrationally excited CO_2 in the plasma volume that produces CO and the cold CO_2 that is also sampled by the IR beam in the gap volumina in front of the KBr side windows. If we assume that the vibrationally excited CO_2 alone exhibits a temperature of the reaction product of CO close to 1200 K one can calculate

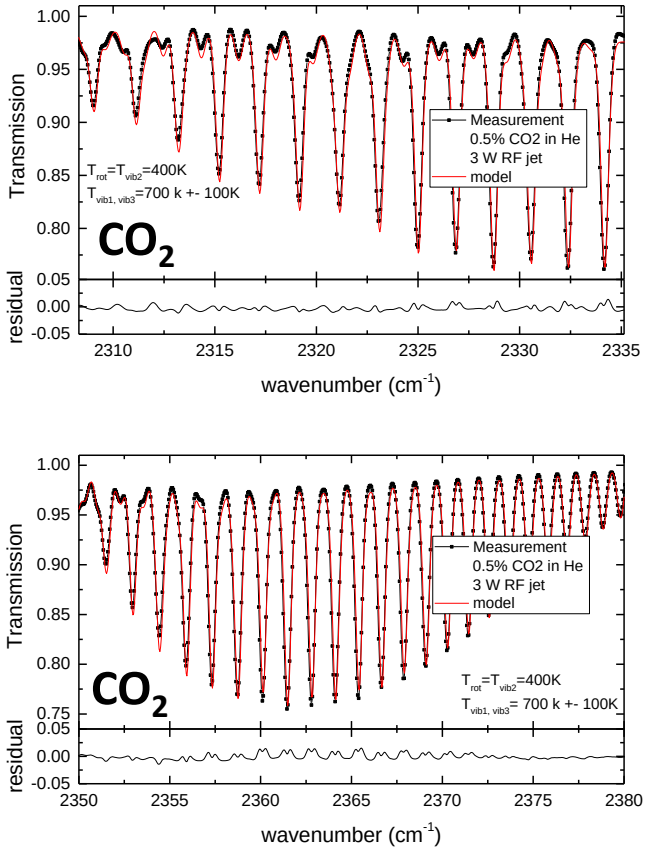

Figure 6. Absorption spectrum of the P branch (upper panel including residuum) and of the R branch (lower panel including residuum) for CO_2 in a plasma jet with 0.5% CO_2 in the feed gas, same data as in Fig. 5.

this average vibrational temperature by comparing the sampling volumina: $T_{average}$= $V_{IR,side}/(V_{IR,side}+V_{IR,central}) \cdot 400$ K + $V_{IR,central}/(V_{IR,side}+V_{IR,central}) \cdot 1200$ K = 760 K. This very rough estimate agrees surprisingly well with the observed range of vibrational temperatures of the stretching vibrations of CO_2.

The rotational and asymmetric stretching vibration temperatures of CO_2 are measured for admixture levels of 0.25%, 0.5%, and 1% for varying absorbed plasma powers between 0.7 W and 3.5 W, as shown in Fig. 10. One can clearly see that the rotational temperature increases slowly with absorbed plasma power, but does not vary significantly with admixture levels. This increase of T_{rot} is fitted to scale linearly with the absorbed power P_{abs} as T_{rot} = 340 K + 80 K $\frac{P_{abs}}{3W}$. The data in Fig. 10 indicate also higher vibrational temperatures for all three CO_2 admixture levels.

The mass balance of the reaction chemistry is assessed by assuming the most simple reaction:

$$CO_2 \rightarrow CO + \frac{1}{2}O_2 \tag{11}$$

The sum of carbon containing species CO and CO_2 partners, as measured by FTIR,

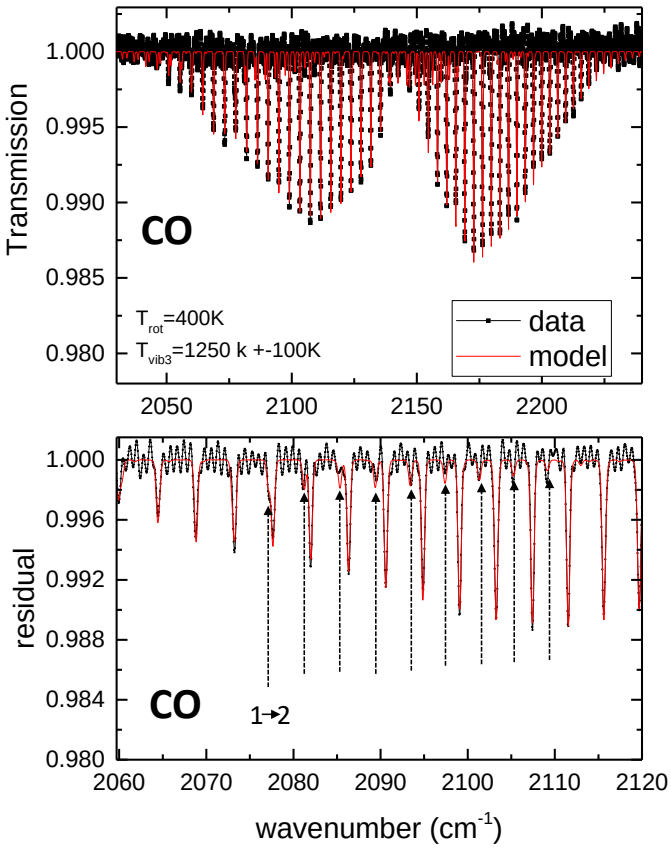

Figure 7. Absorption spectrum of the fundamental of CO generated in a helium plasma jet with 0.5% CO_2 in the feed gas (upper panel). P branch of the absorption spectrum (lower panel), the line positions for the transitions from vibrational states with quantum numbers 1 to states with quantum numbers 2 are indicated.

should stay constant for varying conversion efficiency. The only variation may occur by a temperature variation, which reduces the overall gas density in the reaction volume according to the ideal gas law. The sum of the measured densities of CO and CO_2 for different admixture levels and varying plasma power are shown in Fig. 11. The dashed and solid lines correspond to the gas density of the sum of carbon containing species assuming either a constant temperature of 300 K or assuming the measured neutral gas temperature variation (=rotational temperature) within the plasma region along the optical path (13 mm) and 300 K within the trapped gas region in front of the KBr windows, respectively. In the experiments, we observe a slight increase of the gas temperature with absorbed plasma power. Consequently, the sum of carbon containing species should slightly decrease with increasing plasma power. If the prediction of the temperature dependent total gas density (solid line) is consistent with the measured sum of the CO and CO_2 densities, the mass balance is correct and reaction 11 properly describes the reaction chemistry. The good agreement between data and prediction in Fig. 11 illustrates that the mass balance is correct for all admixture levels and plasma

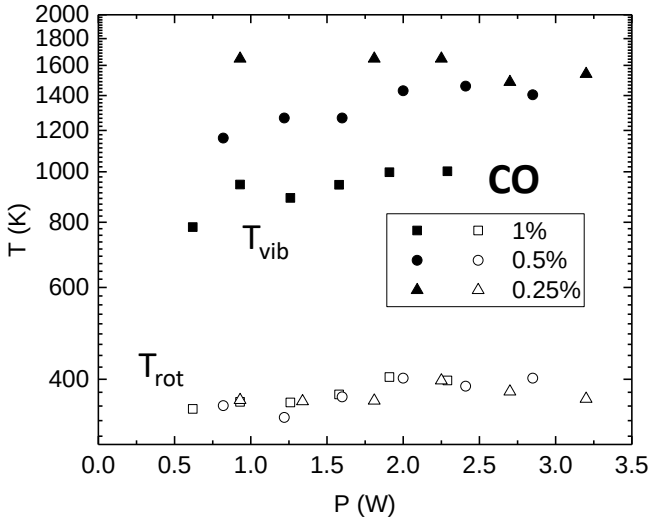

Figure 8. Vibrational and rotational temperatures of CO for varying plasma power and different CO_2 admixture to the helium flow.

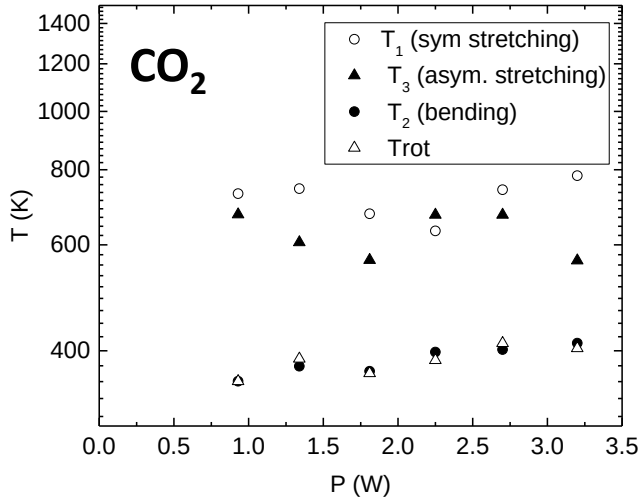

Figure 9. Rotational temperatures and vibrational temperature of CO_2 for varying plasma power and 0.25% CO_2 admixture to the helium flow.

powers in our experiment. This also corroborates the accuracy of the optical modelling of the IR spectra.

The most important quantities to assess the plasma chemistry are the conversion efficiency ϵ and the energy efficiency η of the process. The conversion efficiency ϵ is given as:

$$\epsilon = \frac{n_{CO}}{n_{CO} + n_{CO_2}} \tag{12}$$

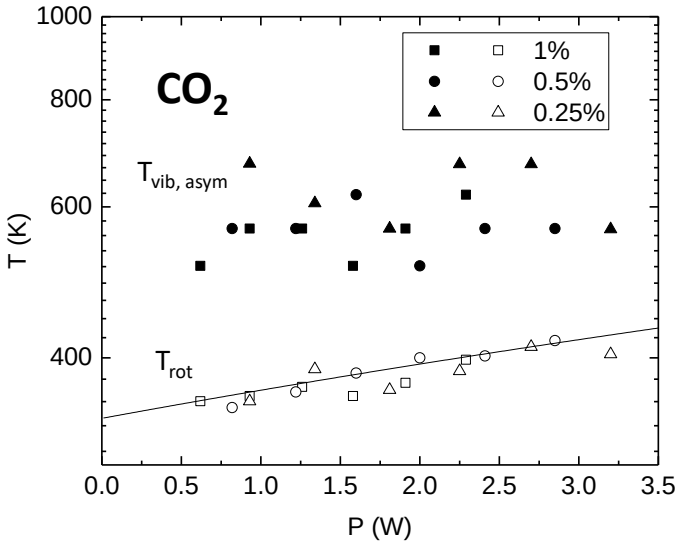

Figure 10. Rotational temperatures and vibrational temperature of the asymmetric stretching vibration of CO_2 for varying plasma power and different CO_2 admixture to the helium flow. The solid line denotes a linear fit according to T_{rot} = 340 K + 80 K $\frac{P_{abs}}{3W}$.

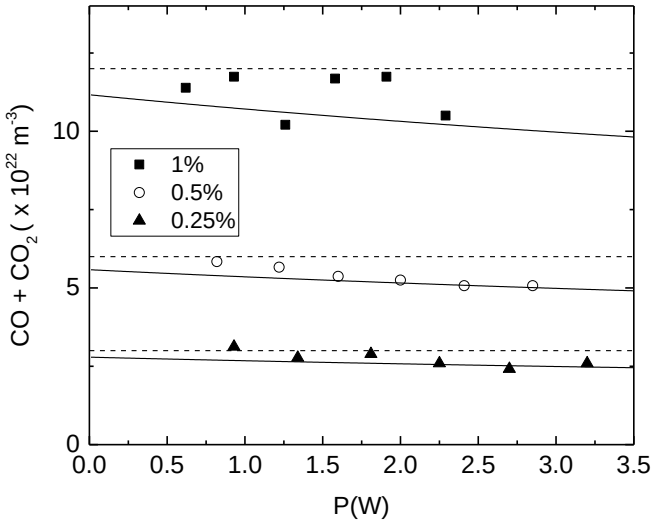

Figure 11. Mass balance of the CO_2 conversion assuming a simple reaction of CO_2 $\rightarrow$ CO + 1/2 O_2 expressed as the total measured density of CO plus CO_2. The dashed lines denote the 100% carbon densities for a given admixture level expected at 300 K. The solid lines denote the expected 100% carbon concentration for an increasing neutral gas temperature (= rotational gas temperature as fitted in Fig. 10)

.

The conversion efficiencies ϵ for varying plasma power and admixture levels are shown in Fig. 12a. The simple reaction 11 of CO_2 $\rightarrow$ CO + 1/2 O_2 can be described by

Admixture	ϵ_∞	SEI
0.25%	30%	29 eV
0.5%	26%	22 eV
1%	20%	19.5 eV

Table 1. Fitting values in eq. 14 for the comparison of the predicted energy and conversion efficiency with the measured data for the three admixture levels. The SEI values are accurate by ± 3 eV and the ϵ_∞ values by ± 5%.

an overall rate constant k with a specific energy input SEI (energy per injected molecule). The general trend of plasma conversion can be expressed as a transition between a *plasma-limited* and a *precursor gas-limited* regime with increasing plasma power. The crossover occurs at a specific plasma power P_{crit} that is sufficient to convert a maximum amount of precursor gas completely into a reaction product. Since the change of the CO_2 density dn_{CO_2} with absorbed plasma power P_{abs} has to obey $\frac{dn_{CO_2}}{dP} \propto -n_{CO_2} P_{abs}$ one can define:

$$\epsilon(P_{abs}) = \epsilon_\infty \left(1 - exp\left(-\frac{P_{abs}}{P_{crit}}\right)\right) \tag{13}$$

This specific power P_{crit} is equal to SEI times the maximum fraction ϵ_∞ of the CO_2 flow $\Phi_{CO_2:He}$ that can be converted [3]. The transition between the *plasma-limited* and the *precursor gas*-limited regime of the conversion efficiency η is then modelled by:

$$\epsilon(P_{abs}) = \epsilon_\infty \left(1 - exp\left(-\frac{P_{abs}}{SEI \cdot \Phi_{CO_2:He} \cdot \epsilon_\infty}\right)\right) \tag{14}$$

with ϵ_∞ the saturation value for the conversion efficiency at very high powers. This equation 14 is used to fit the data, shown as solid lines in Fig. 12a. The fitting values are denoted in table 1. A reasonable agreement between fitting and data is found. A maximum conversion efficiency ϵ_∞ of around 30% is reached, being a bit lower for higher admixture levels. The values for the specific energy input range from SEI = 29 eV for a low admixture level of 0.25% to SEI = 19.5 eV for an admixture level of 1%. It is important to note that the scatter of the data does not allow a very robust fit of SEI and ϵ_∞. A simultaneous lowering or increasing of the value of SEI by 3 eV and of ϵ_∞ by 5% in the fit still yields reasonable agreement between model and data.

In principle, ϵ_∞ should reach 100% at very high plasma powers indicating complete depletion of the source gas (in the limit of extremely high powers the conversion of CO_2 to elemental carbon as wall deposits and O_2 in the outflow should occur). The analysis of the flow pattern of helium and CO_2 showed, however, that this deviation from 100 % is caused by the incomplete mixing of the admixed CO_2 and the plasma volume due to the transport along the complex flow pattern of helium, as discussed above. The diagnostic volume of the IR beam renders even a 100% dissociation degree within the plasma volume as only a CO_2 reduction of 43.5% at maximum. Apparently, only a fraction ϵ_∞ of the CO_2 flow passes the plasma volume and can be dissociated

at maximum. This maximum of 43.5% corresponds to a theoretical upper limit for the fitted values for ϵ_∞. Consequently, a value of $\epsilon_\infty \propto 30\%$ is equivalent to a dissociation degree of 70% in the plasma itself. This effect has to be taken into account, when defining the overall energy efficiency η using the formulas from literature [3]:

$$\eta = \frac{\Delta H}{P_{abs}} \cdot \Phi_{CO_2:He} \cdot \epsilon_\infty \cdot \epsilon \tag{15}$$

with $\Delta H = 2.9$ eV the thermodynamic reaction enthalpy for the dissociation of CO_2, P_{abs} the absorbed plasma power, $\Phi_{CO_2:He} \cdot \epsilon_\infty$ the flow of CO_2 through the plasma volume (5 sccm to 20 sccm). The fit of ϵ is used to predict η by inserting eq. 14 in eq. 15, as shown in Fig. 12b.

4. Discussion

The experiments indicate a non-equilibrium excitation of CO_2 molecules admixed to a high helium gas flow by an RF driven plasma at atmospheric pressure. The strong dilution of CO_2 in helium is an unusual plasma mixture, but seems essential to generate a stable non-equilibrium excitation of the molecules in a cold gas background. A direct comparison can be made to the low pressure experiments by Klarenaar et al. [18], who used a pulsed DC discharge at 3 mbar to excite a pure CO_2 discharge. They found that an equilibrium temperature of about 800 K is reached in the pulsed plasma at 3 ms after the plasma was switched on. The partial pressure of CO_2 in our experiments is of the order of a few mbar for the different admixture levels, which is almost identical to the absolute pressures in the low pressure DC plasma from Klarenaar. The identical CO_2 partial pressure implies an identical mean free path $\lambda_{CO_2-CO_2}$ for CO_2-CO_2 collisions. However, the reaction chemistry along $\lambda_{CO_2-CO_2}$ in the *low pressure pulsed DC plasma* and the *atmospheric pressure helium diluted RF jet* are very different: (i) *low pressure pulsed DC plasma*: no collisions with other species occur along $\lambda_{CO_2-CO_2}$ and CO_2 may only be excited by plasma electrons or de-excite via radiation. The power density can be estimated from the plasma volume and voltage and current value, as given by Klarenaar et al. [18] yielding 1 W cm^{-3}; (ii) *atmospheric pressure helium diluted RF jet*: CO_2 is embedded in a cold fast flowing helium gas containing also excited helium metastables or dimers. The typical power density can be estimated from the absolute powers up to 3 W and a plasma volume of 0.34 cm^{-3} (1 mm × 13 mm × 26 mm), yielding approximately 9 W cm^{-3}. The higher power density should imply also a higher electron density compared to the DC plasma case and, therefore, also more efficient excitation along $\lambda_{CO_2-CO_2}$. The de-excitation via radiation is similar to the low pressure case. In addition, rotationally and vibrationally excited CO_2 is efficiently quenched in collisions with helium along $\lambda_{CO_2-CO_2}$ via VT-relaxation [22], which explains the slight increase in the rotational temperature to 400 K with increasing plasma power. This VT-relaxation is, however, in competition with excitations via Penning collision of CO_2 with helium metastables and dimers. Such Penning collisions correspond to an electronic excitation of CO_2 that populate preferably the asymmetric stretching vibration [5].

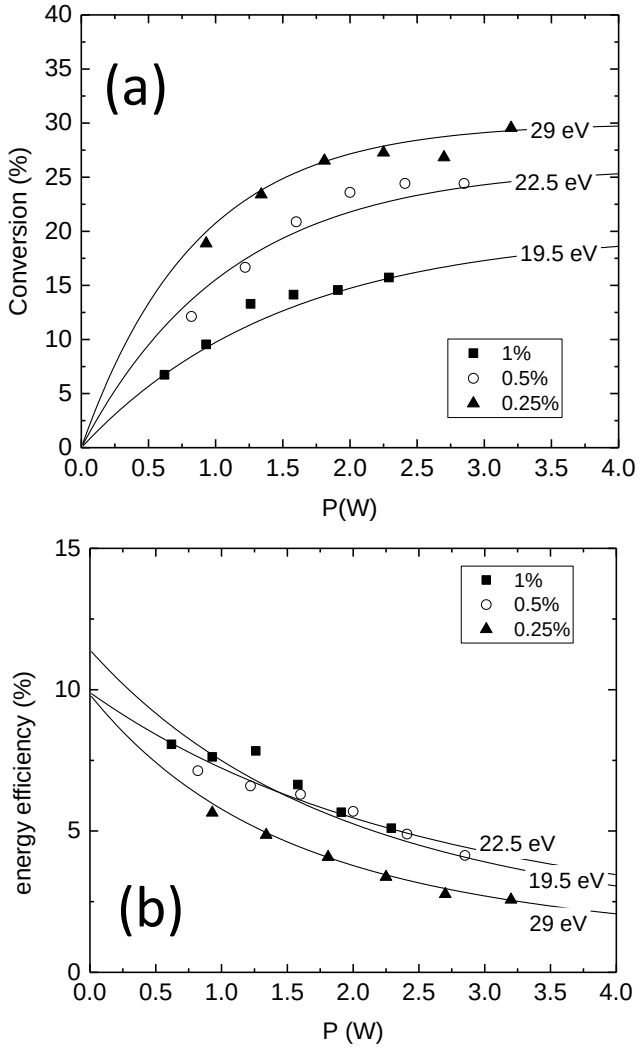

Figure 12. Conversion efficiency (a) and energy efficiency (b) for three different admixture levels at varying plasma power. The solid line in (a) corresponds to a simple model for a transition between a *plasma-limited* to a *precursor gas-limited* regime with increasing plasma power according to equation 14 (the fitted SEI values are indicated). The solid lines in (b) models the energy efficiency according to the solution of the fitted equation 14 inserted into eq. 15 (the fitted SEI values are indicated).

This postulated reaction scheme is highlighted in Fig. 13 for the excitation of He (a) and for the reaction channels of CO_2 dissociation (b) for a 1% admixture of CO_2 in helium: the power is at first absorbed by the electrons in the plasma. Since the majority of the collision partners are helium atoms, they are at first excited either via creation of a metastable He $^3S_1$ with a threshold of 19.82 eV or via creation of an He^+ ion with an energy threshold of 24.8 eV. These metastables may exchange their energy in resonant collisions with other helium atoms in the ground state or they may recombine in three body collisions in forming helium dimers He_2. 1% of the collision partners

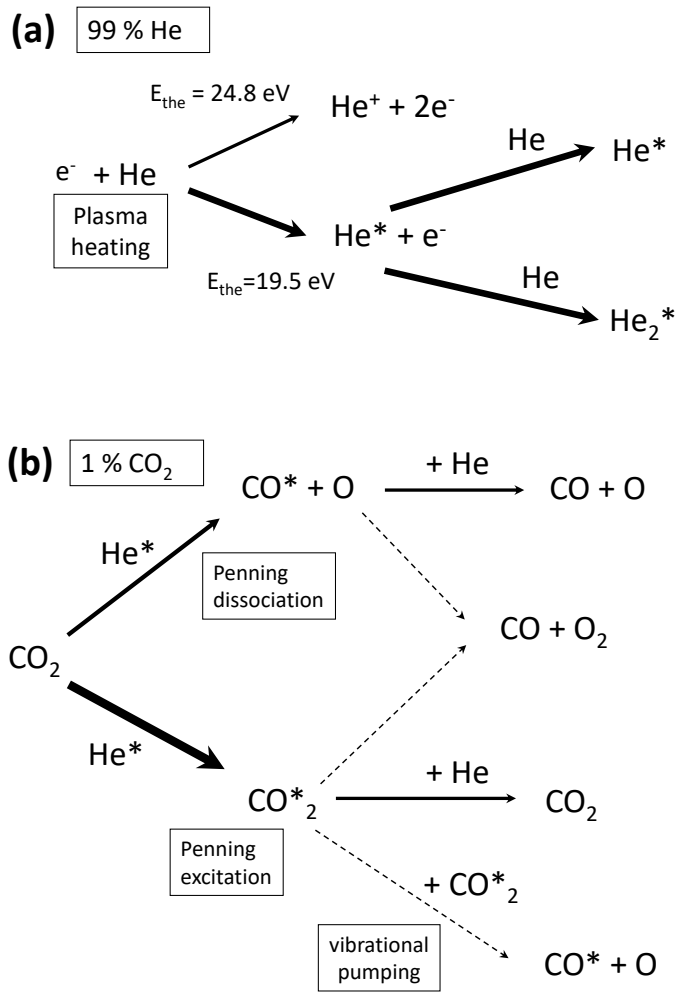

Figure 13. Postulated reaction sequence of CO_2 dissociation vai collisions with excited helium species, (a) helium excitation, (b) CO_2 excitation and dissociation.

of these excited He species are CO_2 species in the ground state leading to Penning excitation of CO_2. This corresponds to electronic excitation of CO_2, which may lead either into excitation to CO_2^* or to dissociative excitation to CO^*+O. This electronic excitation via Penning collisions preferably creates vibrationally excited molecules due to the Frank-Condon principle. These excited molecule may then quench via collisions with ground state He leading to a VT relaxation. The average population, expressed as a temperature for the population of the lower vibrational mode is then a results between the excitation by Penning collisions with excited helium species and VT relaxation by collisions with He ground state species. The observed SEI values of 20 eV and above are consistent with a main dissociation mechanism consisting of helium metastable excitation by electrons with energies of 20 eV and above followed by the excitation transfer from helium metastables to CO_2 that results in dissociation and generation of vibrationally excited CO molecules. An SEI around 20 eV compared to the reaction

enthalpy of 2.9 eV for CO_2 dissociation is consistent with the observation of an energy efficiency up to 10 %.

The use of CO_2 (or other molecules) diluted in fast flowing helium plasma jets is well suited for the analysis of plasma catalysis systems. These types of plasmas are obviously able to generate non-equilibrium populations consisting of vibrationally excited molecules, but with small translational and rotational temperatures. This avoids any unintentional plasma heating of a catalyst surface. Consequently, the impact of *only* vibrationally excited molecules on the efficiency of a specific plasma catalysis surface process can be tested. In preliminary experiments, we already observed an enhancement of the reduction of CO_2 when comparing plasma conversion with and without a silica supported nickel-oxide catalyst operated at room temperature. This catalyst requires usually a surface temperature in the range of 800 K in conventional thermal catalysis. Apparently, the surface reaction of excited CO_2 on this nickel-oxide catalyst is already efficient at low temperatures. This will be analysed in more depth in the future.

5. Conclusion

A strong non-equilibrium for the excitation of CO_2 and CO in helium diluted RF plasma jets has been found. Whereas the rotational temperature is 400 K or below, the vibrational temperature for CO reaches values up to 1400 K and that of the asymmetric stretching vibration of CO_2 of 800 K. This non-equilibrium is explained by the nature of the excitation of the molecules by Penning collisions with excited helium metastables or dimers. The helium plasma gas acts apparently as a buffer to maintain a cold rotational gas temperature. This non-equilibrium character makes these plasmas an ideal candidate to study any synergisms in plasma catalysis, where one has to assure that any enhancement of a reaction rate should occur only by the contribution of surface reactions with excited molecules and not due to an unintentional heating of the catalyst surface by the plasma itself.

Acknowledgements

This project is supported by the BMBF in the framework of the L3 subproject of the Carbon2Chem consortium and by the DFG (German Science Foundation) within the framework of the Coordinated Research Centre SFB 1316 at Ruhr-University Bochum. The authors relied on the contributions of Sarah Klose and Simon Hübner ,who performed the initial experiments of the project. Finally, valuable discussions with Bert Klarenaar and Richard Engeln are acknowledged.

References

[1] Bogaerts A, Kozák T, van Laer K and Snoeckx R 2015 *Faraday Discussions* **183** 217–232 ISSN 1359-6640, 1364-5498

[2] Chen G, Godfroid T, Britun N, Georgieva V, Delplancke-Ogletree M P and Snyders R 2017 *Applied Catalysis B: Environmental* **214** 114–125 ISSN 09263373
[3] Heijkers S, Snoeckx R, Kozák T, Silva T, Godfroid T, Britun N, Snyders R and Bogaerts A 2015 *The Journal of Physical Chemistry C* **119** 12815–12828 ISSN 1932-7447, 1932-7455
[4] van Rooij G J, van den Bekerom D C M, den Harder N, Minea T, Berden G, Bongers W A, Engeln R, Graswinckel M F, Zoethout E and van de Sanden M C M 2015 *Faraday Discussions* **183** 233–248 ISSN 1359-6640, 1364-5498
[5] Fridman A A 2008 *Plasma Chemistry* (Cambridge: Cambridge University Press)
[6] Rusanov V D, Fridman A A and Sholin G V 1981 *Sov. Phys. Usp.* **24** 447
[7] Neyts E C, Ostrikov K K, Sunkara M K and Bogaerts A 2015 *Chemical Reviews* **115** 13408–13446 ISSN 0009-2665, 1520-6890
[8] Neyts E C and Bogaerts A 2014 *Journal of Physics D: Applied Physics* **47** 224010 ISSN 0022-3727, 1361-6463
[9] Whitehead J C 2016 *Journal of Physics D: Applied Physics* **49** 243001 ISSN 0022-3727
[10] Golda J, Held J, Redeker B, Konkowski M, Beijer P, Sobota A, Kroesen G, Braithwaite N S J, Reuter S, Turner M M, Gans T, O'Connell D and Schulz-von der Gathen V 2016 *Journal of Physics D: Applied Physics* **49** 084003 ISSN 0022-3727, 1361-6463
[11] Waskoenig J, Niemi K, Knake N, Graham L M, Reuter S, Schulz-von der Gathen V and Gans T 2010 *Pure and Applied Chemistry* **82** 1209–1222 ISSN 1365-3075, 0033-4545
[12] Waskoenig J, Niemi K, Knake N, Graham L M, Reuter S, der Gathen V S v and Gans T 2010 *Plasma Sources Science and Technology* **19** 045018 ISSN 0963-0252, 1361-6595
[13] Horn K P and Oettinger P E 1971 *The Journal of Chemical Physics* **54** 3040–3046 ISSN 0021-9606, 1089-7690
[14] Plo E and Rich J W 2000 *E. Pl* 17
[15] Rothman L, Jacquemart D, Barbe A, Chris Benner D, Birk M, Brown L, Carleer M, Chackerian C, Chance K, Coudert L, Dana V, Devi V, Flaud J M, Gamache R, Goldman A, Hartmann J M, Jucks K, Maki A, Mandin J Y, Massie S, Orphal J, Perrin A, Rinsland C, Smith M, Tennyson J, Tolchenov R, Toth R, Vander Auwera J, Varanasi P and Wagner G 2005 *Journal of Quantitative Spectroscopy and Radiative Transfer* **96** 139–204 ISSN 00224073
[16] Rothman L 1998 *J. Quant. Spectrosc. Radiat. Transfer* **60** 665
[17] Šimečková M, Jacquemart D, Rothman L S, Gamache R R and Goldman A 2006 *Journal of Quantitative Spectroscopy and Radiative Transfer* **98** 130–155 ISSN 00224073
[18] Klarenaar B L M, Engeln R, van den Bekerom D C M, van de Sanden M C M, Morillo-Candas A S and Guaitella O 2017 *Plasma Sources Science and Technology* **26** 115008 ISSN 1361-6595
[19] Nairmen M, Manzanares C and Caballero J 1996 *J. Chem. Education* **73** 804
[20] Mader H, Guarnieri A, Doose J, Nissen N, Markov V N, Shtanyuk A M, Andrianov A F, Shanin V N and Krupnov A F 1996 5
[21] Sinclair P, Duggan P, Berman R, Drummond J R and May A 1998 *Journal of Molecular Spectroscopy* **191** 258–264 ISSN 00222852
[22] Yardley J 1980 *Introduction to Molecular Energy Transfer* (New York: Academic Press)